Engineering Solid Mechanics 13 (2025) 125-140

Contents lists available at GrowingScience

Engineering Solid Mechanics

homepage: www.GrowingScience.com/esm

Exploring stress intensity factor computation: A parametric study using extended isogeometric analysis (XIGA)

Migbar Assefa Zeleke[a*], Mesfin Belayneh Ageze[b], Ntirelang Robert Batane[a], Edward Dintwa[a]

[a]*Department of Mechanical Engineering, University of Botswana, Botswana*
[b]*Center for Renewable Energy, Addis Ababa Institute of Technology, Addis Ababa University, Addis Ababa, Ethiopia*

A R T I C L E I N F O

Article history:
Received 8 April 2024
Accepted 26 June 2024
Available online
26 June 2024

Keywords:
Stress intensity factor
Fracture mechanics
Non-Uniform Rational B-Splines(NURBS)
Isogeometric Analysis (IGA)
Extended Isogeometric Analysis (XIGA)

A B S T R A C T

The permanence and durability of mechanical and structural elements with discontinuities such as cracks and voids require the calculation of SIF (stress intensity factors) with reasonable fidelity. SIF is a crucial parameter that predicts crack growth and failure behavior by quantifying the stress field neighboring the crack tip. Therefore, understanding the sophisticated characteristics of the stress fields in the vicinity of discontinuity requires an effective way of calculating SIFs. Currently, there are numerous methods to calculate SIF, such as FVM (Finite Volume Method), FEM (Finite Element Method), BEM (Boundary Element Method), XFEM (Extended Finite Element Method), Phase field method and Meshfree methods. For an extended period, FEM is one of the leading methods in solving fracture mechanics problems. Though FEM is quite robust in dealing with several engineering problems, it has got its inherent drawbacks to deal with singular fields like discontinuities. Hence to reasonably capture moving discontinuities, finer meshes near the discontinuous field are required that demand more computation effort and time. To alleviate the above drawback of FEM, this study employed Extended Isogeometric Analysis (XIGA) to efficiently and effectively determine the SIFs in the case of fissured plates as benchmarking fissure problems. In this study SIFs in relation to crack length were examined for edge and center cracked plates and results were compared with the theoretical values.

Nomenclature

SIF	stress intensity factors	Γ_c	Traction free boundary
FVM	Finite Volume Method	Γ_u	Displacement surface traction
FEM	Finite Element Method	σ	Cauchy stress tensor
BEM	Boundary Element Method	b	body force per unit volume
XFEM	Extended Finite Element Method	$\bar{t}$	traction vector
XIGA	Extended Isogeometric Analysis	D	Constitutive matrix.
IGA	Isogeometric Analysis	ε	Strain tensors
ξ_i	the i^{th} knot, i represents the knot index,	K	Global stiffness matrix,
P	the order of the polynomial	f	The force vector
n	the number of basis functions	u	Displacement vector
N_i	An i^{th} B-spline basis functions	J	Jacobian matrix
$P(\xi)$	The curves of the Rational B-spline	$H(\xi)$	Heaviside function
B_i	Control points	β_α	Crack tip enrichment functions.
R_i	NURBS basis function	a_j	Extra degrees of freedom for crack face
w_i	Weights of the control points	b_k^α	Extra degrees of freedom for crack tip
Γ_t	Traction surface		
NURBs	Non-Uniform Rational B-Splines		

* Corresponding author.
E-mail addresses: zelekem@ub.ac.bw (M. A. Zeleke)

ISSN 2291-8752 (Online) - ISSN 2291-8744 (Print)

doi: 10.5267/j.esm.2024.6.003

1. Introduction

Fracture is a critical failure mode in engineering and responsible for structural failure of many catastrophic accidents in various engineering installations result from the presence of defects like micro-cracks and voids. Therefore, a deep understanding of fracture mechanics is crucial. The determination of SIFs is recognized as a significant accomplishment in the domain of LEFM (Linear Elastic Fracture Mechanics). The concept of SIF was initially introduced by Irwin in 1957 Irwin (1957), building upon the work of Griffith (1921). Irwin's research revealed that the SIF is a critical parameter that characterizes the stress field near the crack tip. Through his research, Irwin uncovered the significance of SIFs as central parameters that delineate the stress state in the neighborhood of crack tip. SIF also provides information about the direction and speed of crack propagation, making it useful for determining crack growth rate. The SIF depends on factors such as crack size, crack location, specimen geometry, and the magnitude and distribution of the applied load (Pais, 2011). Understanding this important parameter allows for predicting crack growth rate and residual strength of damaged structures, ensuring the safe operation of machines and structural components despite surface and internal flaws Kastratovic et al. (2018). Numerous approaches have been devised to ascertain SIFs, encompassing analytical solutions, experimental methodologies, and numerical techniques. A very good account of the analytical and finite element-based methods was compiled by Sih (1973). Analytical solutions are tend to focus on simple crack geometries and loading conditions, and they often rely on idealized assumptions that may not accurately represent real-world situations Tada et al. (2000). Experimental methods involve measuring parameters such as crack opening displacements or crack growth rates under controlled loading conditions. While these methods provide valuable data, they can be time-consuming and costly, especially when dealing with complex geometries or high-stress environments.

Numerical techniques, such as FEM, have become increasingly popular for determining SIFs. The FEM enables the modeling of intricate crack geometries and loading conditions, thereby offering realistic depiction of practical situations. By dividing the structure into finite elements and solving the governing equations, FEM has the competence to calculate SIF but encounters challenges, including mesh generation, accurate crack modeling, and precise extraction of the stress singularity. To circumvent the above challenges of FEM, advanced computational techniques like XFEM, Belytschko and Black (1999); Moes et al. (1999); Menk and Bordas (2011); Singh et al. (2012); Bouhala et al. (2013); Zeleke et al. (2021) phase field method, Miehe et al., (2010, a); Miehe et al., (2010, b); Borden et al., (2012), Isogeometric Analysis (IGA), Hughes et al. (2005), Nguyen et al. (2015) and Meshfree methods, Belytschko et al. (1994, a), Belytschko et al. (1994, b), Lu et al. (1994), Liu et al. (1995), Rabczuk and Belytschko (2004), Ching and Yen (2005), Gu et al., (2011), Lee et al. (2016) have been employed. XIGA has emerged as a powerful alternative to the finite element method (FEM) for solving fracture mechanics problems. While FEM is a robust technique, it struggles to accurately capture singular fields and discontinuities, requiring fine meshes that increase computational demands. To address this limitation, this study employed XIGA to efficiently and effectively determine stress intensity factors (SIFs) for cracked plates. The investigation examined SIFs in relation to crack length for both edge-cracked and center-cracked plates, and the results were compared against theoretical values.

1.1 Isogeometric Analysis

Isogeometric analysis (IGA) is a computational technique that integrates CAD with FEA to enhance the precision and effectiveness of numerical simulations. Hughes and his colleagues introduced IGA as a novel computational mechanics approach in 2005 (Hughes et al., 2005). Traditionally, FEA uses polynomial approximations, like linear or quadratic elements, to represent the geometry of an object or structure, while CAD systems rely on NURBS or other spline representations for complex shapes. The aim of IGA is to bridge the gap among CAD and FEA by employing identical basis functions such as NURBS, to represent the geometry and approximate the solution fields in FEA. This eliminates the need for geometric conversion or approximation steps, as the same geometry representation can be used for both design and analysis.

Since its introduction, IGA has had a significant impact on the field of computational mechanics. Its integration of CAD and FEA has stimulated advancements in geometric modeling and numerical simulation. The method has gained widespread adoption and citation in numerous research papers, conference proceedings, and books. It's potential to enhance accuracy and efficiency in numerical simulations, particularly for problems involving complex geometries, has attracted considerable attention from the scientific community. Over the years, IGA has found applications in various disciplines, including structural mechanics, fluid dynamics, electromagnetics, and multiphysics problems. Its ability to seamlessly integrate CAD and FEA has made it an appealing choice for researchers and engineers working on problems with geometric complexities. **Fig. 1** and **Fig. 2** below illustrate the increasing trend in the number of published articles and citations received between 2006 and 2024, showcasing the growing significance of IGA in the field.

In the past decade, several studies have employed XIGA to address various engineering problems. Gu et al. (2019) developed an adaptive XIGA approach to investigate fracture mechanics of cracked orthotropic composite structures. Yang et al. (2020) used XIGA based on PHT-splines to study vibration and buckling of functionally graded material plates with cracks and cutouts. Bhardwaj et al. (2021) employed XIGA for thermo-elastic analysis of cracks in functionally graded materials. Later, Fang et al. (2021) utilized an adaptive XIGA approach to investigate the thermal buckling of functional graded plates with flaws. Recently, Shoheib (2023) proposed XIGA using NURBS-based Bezier extraction to evaluate stress intensity factors for surface cracks in pipeline welds. Very recently, Zhong et al. (2024) developed a 3D rotating cracked blade model using XIGA with enriched elements to represent crack surfaces and singularities.

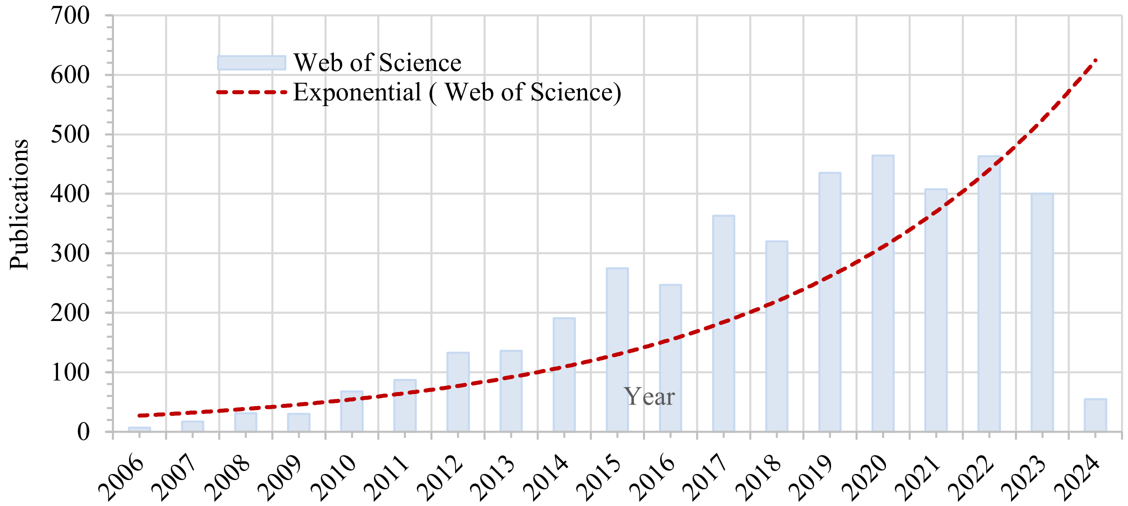

Fig. 1 Number of IGA Articles (2006-2024) (Source: web of science database).

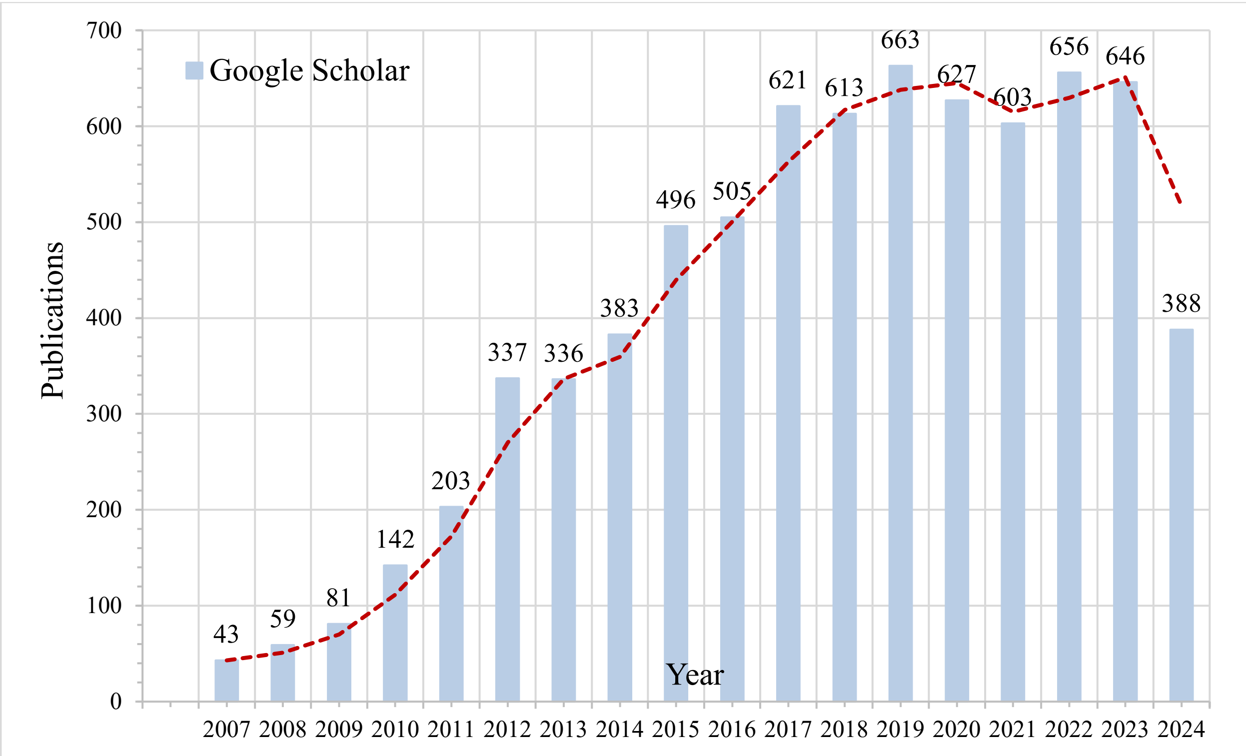

Fig. 2. Number of Citations of Hughes et al., (2005) (2006-2024) (Source: Google Scholar).

2. Numerical implementation and Governing Equations

2.1 Basis Function

B-spline is a type of curve that is represented by a collection of control points and is created using piecewise polynomial functions. Unlike interpolating curves, B-splines do not require to pass through all the control points. Rather, they are determined by a collection of control points that impact the overall shape of the curve. B-spline curve is constructed using a sequence of polynomial basis functions, each possessing a specific degree.

In this section, we will provide a brief explanation of B-spline basis functions. The computation of these basis functions often employs the recursion formula of Cox-de Boor. To create a B-pline, the initial step is to define a knot vector Ξ that represents a sequence of parameter values arranged in ascending order and is determined by a set of coordinates, which can be expressed as follows (Hughes et al., 2005; Nguyen et al., 2015; Jameel & Harmain, 2019; Ghorashi et al., 2012):

$$\Xi = \{\xi_1, \xi_2, \dots \xi_{n+p+1}\} \tag{1}$$

where $\xi_i (i = 1,2, \cdots\cdots n + p + 1)$ symbolizes the i^{th} knot, n designates the number of basis functions, p signifies polynomial order and i represents the knot index. Now we can define the shape functions in a recursive manner for $p = 0$ as follows (Hughes et al., 2005; Nguyen et al., 2015; Jameel & Harmain, 2019; Ghorashi et al., 2012):

$$N_{i,0}(\xi) = \begin{cases} 1, \text{ } if \text{ } \xi \in [\xi_i, \xi_{i+1}] \\ 0, \quad otherwise \end{cases} \tag{2}$$

and for $p \geq 1$

$$N_{i,p}(\xi) = \frac{\xi - \xi_i}{\xi_{i+p} - \xi_i} N_{i,p-1}(\xi) + \frac{\xi_{i+p+1} - \xi}{\xi_{i+p+1} - \xi_{i+1}} N_{i+1,p-1}(\xi) \tag{3}$$

Eq. (3) is known as the recursion formula of Cox de Boor.

The derivatives of the basis function are Ghorashi et al., (2012):

$$\frac{dN_{i,p}(\xi)}{d\xi} = \frac{p}{\xi_{i+p} - \xi_i} N_{i,p-1}(\xi) + \frac{p}{\xi_{i+p+1} - \xi_{i+1}} N_{i+1,p-1}(\xi) \tag{4}$$

The curves of the Rational B-spline are determined by $n+1$ control points and given as:

$$P(\xi) = \sum_{i=0}^{n} B_i R_{i,p}(\xi) \tag{5}$$

where $B_i[X_i, Y_i]$ represents the control points' coordinates in 2-D and $R_{i,p}(\xi)$ are NURBS shape function and given as:

$$R_{i,p}(\xi) = \frac{w_i N_{i,p}(\xi)}{W(\xi)} = \frac{w_i N_{i,p}(\xi)}{\sum_{i=0}^{n} w_i N_{i,p}(\xi)} \tag{6}$$

where w_i denotes control points' weights and $N_{i,p}(\xi)$ are the B-spline shape function of the p^{th} order.

2.2 Isogeometric discretization

Consider a 2-D domain Ω confined by the surface Γ as shown in **Fig. 3**. The boundary is segmented in to traction surface Γ_t, traction free boundary Γ_c and the displacement surface traction boundary Γ_u.

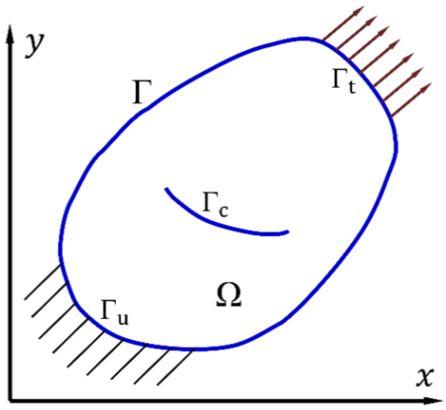

Fig. 3. A two-dimensional continuum with boundary and loading conditions

The equilibrium equation along with the BCs for any deformable can be written as

$$\nabla \cdot \boldsymbol{\sigma} + \mathbf{b} = 0 \quad \text{in } \Omega \tag{7}$$

$$\boldsymbol{\sigma} \cdot \mathbf{n} = \bar{\mathbf{t}} \quad \text{on } \Gamma_t \tag{8}$$

$$\boldsymbol{\sigma}\cdot\mathbf{n}=0 \quad \text{on } \Gamma_c \tag{9}$$

where; $\boldsymbol{\sigma}$ represents Cauchy stress tensor, b denotes body force per unit volume and $\bar{\mathbf{t}}$ represents traction vector. For elastic material the stress and strain tensors are related by

$$\boldsymbol{\sigma}=\mathbf{D}\boldsymbol{\varepsilon} \tag{10}$$

where $\mathbf{D}$ represents the material matrix. The weak form of Eq. (7) is written as

$$\int_{\Omega}\boldsymbol{\sigma}:\boldsymbol{\varepsilon}\,d\Omega=\int_{\Omega}\mathbf{b}:\mathbf{u}\,d\Omega+\int_{\Gamma_t}\bar{\mathbf{t}}:\mathbf{u}\,d\Gamma_t \tag{11}$$

Discretization of Eq. (11) results:

$$[\mathbf{K}]\{\mathbf{u}\}=\{\mathbf{f}\} \tag{12}$$

In the provided context, the global stiffness matrix, force vector, and displacement vector are represented by the symbols K, f, and u, respectively. To obtain the force vector f and stiffness matrix K, they are formed by combining the element force vector and the element stiffness matrix according to the following technique:

$$\mathbf{K}_{\mathbf{e}}=\int_{\boldsymbol{\Omega}_{\mathbf{e}}}(\mathbf{B})^{\mathrm{T}}\mathbf{D}\mathbf{B}\,d\Omega \tag{13}$$

$$\mathbf{f}_{\mathbf{e}}=\int_{\boldsymbol{\Omega}_{\mathbf{e}}}(\mathbf{R})^{\mathrm{T}}\mathbf{b}\,d\Omega-\int_{\Gamma_{\mathbf{t_e}}}(\mathbf{R})^{\mathrm{T}}\bar{\mathbf{t}}\,d\Gamma \tag{14}$$

$\mathrm{R}(\xi)$ denotes vector of NURBS shape functions $\mathrm{R_i}, (\mathrm{i}=1,2,\cdots\cdots,\mathrm{n_{en}})$ in the domain of $\xi=(\xi_1,\xi_2)$ and are elucidated in the form of B-matrix as:

$$\mathrm{B}=\begin{bmatrix}\dfrac{\partial \mathrm{R}_1}{\partial \mathrm{X}_1} & 0 & \cdots & \dfrac{\partial \mathrm{R}_{\mathrm{n_{en}}}}{\partial \mathrm{X}_1} & 0\\ 0 & \dfrac{\partial \mathrm{R}_1}{\partial \mathrm{X}_2} & \cdots & 0 & \dfrac{\partial \mathrm{R}_{\mathrm{n_{en}}}}{\partial \mathrm{X}_2}\\ \dfrac{\partial \mathrm{R}_1}{\partial \mathrm{X}_2} & \dfrac{\partial \mathrm{R}_1}{\partial \mathrm{X}_1} & \cdots & \dfrac{\partial \mathrm{R}_{\mathrm{n_{en}}}}{\partial \mathrm{X}_2} & \dfrac{\partial \mathrm{R}_{\mathrm{n_{en}}}}{\partial \mathrm{X}_1}\end{bmatrix} \tag{15}$$

The number of DOF is represented by $n_{en}=(p+1)\times(q+1)$. The variables p and q represent the curve orders in the ξ_1 *and* ξ_2 directions, respectively. The displacement representation u^h and spatial coordinates $X=(X_1,X_2)$ are obtained for a specific point $\xi=(\xi_1,\xi_2)$ in parametric coordinates as follows (Ghorashi et al. 2012):

$$u^h(\xi)=\sum_{i=1}^{n_{en}}R_i(\xi)u_i \tag{16}$$

$$X(\xi)=\sum_{i=1}^{n_{en}}R_i(\xi)B_i \tag{17}$$

where $\mathrm{u_i}$ denotes value of the $\mathrm{i^{th}}$ component of the vector u, derived from the solution of Eq. (12). Before calculating the spatial derivatives of basis functions R_{i,X_1} and R_{i,X_2} it is essential to compute the Jacobian matrix (J) as:

$$J=\begin{bmatrix}\dfrac{\partial X_1}{\partial \xi_1} & \dfrac{\partial X_2}{\partial \xi_1}\\ \dfrac{\partial X_1}{\partial \xi_2} & \dfrac{\partial X_2}{\partial \xi_2}\end{bmatrix} \tag{18}$$

The shape functions' derivative with respect to the spatial coordinates can be found using the following procedure:

(19)

$$\begin{Bmatrix} \dfrac{\partial R_i}{\partial X_1} \\ \dfrac{\partial R_i}{\partial X_2} \end{Bmatrix} = J^{-1} \begin{Bmatrix} \dfrac{\partial R_i}{\partial \xi_1} \\ \dfrac{\partial R_i}{\partial \xi_2} \end{Bmatrix}$$

2.3 Extended Isogeometric Analysis (XIGA)

XIGA extends the capabilities of IGA by introducing additional enrichment techniques to address crack modeling and stress singularity factor computations. The enrichment functions are introduced to improve the representation of crack behavior and accurately capture stress concentrations near crack tips. Inspired by the XFEM enrichment functions (Belytschko & Black, 1999; Moes et al., 1999), such as the generalized Heaviside functions, XIGA can be employed to accurately model crack growth problems.

2.4 XIGA approximations for cracks

The estimation of the displacement field within the framework of XIGA can be presented as follows to model crack edges and tips De Luycker et al., (2011):

$$u^h(\xi) = \sum_{i=1}^{n_{en}} R_i(\xi) u_i + \underbrace{\sum_{j=1}^{n_{cf}} R_j(\xi) H(\xi) a_j}_{\text{crack face enrichment}} + \underbrace{\sum_{k=1}^{n_{ct}} R_k(\xi) \left(\sum_{\alpha=1}^{4} \beta_\alpha(\xi) b_k^\alpha \right)}_{\text{crack tip enrichment}} \tag{20}$$

where $H(\xi)$ represents the Heaviside function, while β_α denotes the crack tip enhancement functions. Vectors a_j and b_k^α represents the additional DOF linked to the modeling of the crack face and crack tip, respectively. The n_{cf} corresponds to number of n_{en} basis functions that solely encompass the crack face within their support domain and n_{ct} denotes the count of basis functions that are related to the crack tip within their influential domain. The Heaviside function, denoted as $H(\xi)$, takes on a value of +1 when the physical space that correspond to the natural coordinates ξ are positioned above the crack, and on the opposite side of the crack discontinuity, it takes -1. According to Moes et al. (1999) the Heaviside function is given by:

$$H(x) = \begin{cases} +1, \; if \; (x - x^*) \cdot n \geq 0 \\ -1, \; otherwise \end{cases} \tag{21}$$

The crack tip enrichment functions, as defined in reference (Moes, et al., (1999), are used to enhance the representation of the crack tip.

$$\beta(r,\theta) = [\beta_1, \beta_2, \beta_3, \beta_4] = \left[\sqrt{r}\left(\sin\frac{\theta}{2}\right), \sqrt{r}\left(\cos\frac{\theta}{2}\right), \sqrt{r}\left(\sin\frac{\theta}{2}\right)\cos\theta, \sqrt{r}\left(\cos\frac{\theta}{2}\right)\cos\theta \right] \tag{22}$$

In the local coordinate system of the crack front, the polar coordinates are represented by r and θ. These coordinates describe the position of points relative to the crack and can be determined using the following expression:

$$\begin{cases} r = \sqrt{x_1^2 + x_2^2} \\ \theta = \arctan\left(\dfrac{x_2}{x_1}\right) \end{cases} \tag{23}$$

The coordinates in the local Cartesian system at the crack tip is denoted as (x_1, x_2), correspond to the crack tip position $X_{tip}(X_{1_{tip}}, X_{2_{tip}})$.

$$\begin{Bmatrix} x_1 \\ x_2 \end{Bmatrix} = \begin{bmatrix} \cos\varphi & \sin\varphi \\ -\sin\varphi & \cos\varphi \end{bmatrix} \begin{Bmatrix} X_1 - X_{1_{tip}} \\ X_2 - X_{2_{tip}} \end{Bmatrix} \tag{24}$$

In Eq. (20), the first term on the right-hand side calculates the displacement field using the classical approximation in Isogeometric Analysis (IGA). The remaining terms serve as enrichments to accurately model a crack. When dealing with a crack, the matrices k and f in Eq. (12) are derived by utilizing the approximation function defined in Eq. (20) as

$$K_{ij}^{e}=\begin{bmatrix} K_{ij}^{uu} & K_{ij}^{ua} & K_{ij}^{ub} & K_{ij}^{uc} & K_{ij}^{ud} \\ K_{ij}^{au} & K_{ij}^{aa} & K_{ij}^{ab} & K_{ij}^{ac} & K_{ij}^{ad} \\ K_{ij}^{bu} & K_{ij}^{ba} & K_{ij}^{bb} & K_{ij}^{bc} & K_{ij}^{bd} \\ K_{ij}^{cu} & K_{ij}^{ca} & K_{ij}^{cb} & K_{ij}^{cc} & K_{ij}^{cd} \\ K_{ij}^{du} & K_{ij}^{da} & K_{ij}^{db} & K_{ij}^{dc} & K_{ij}^{dd} \end{bmatrix} \tag{25}$$

$$f^{e}=\{f_i^{u} \quad f_i^{a} \quad f_i^{b1} \quad f_i^{b2} \quad f_i^{b3} \quad f_i^{b4} \quad f_i^{c} \quad f_i^{d}\}^{T} \tag{26}$$

$$K_{ij}^{rs}=\int_{\Omega^e}(B_i^r)^T C(B_j^s)\, d\Omega\,, (r,s=u,a,b,c,d) \tag{27}$$

$$f_i^u=\int_{\Omega^e}R_i^T b\, d\Omega+\int_{\Gamma_t}R_i^T\bar{t}\, d\Gamma, \tag{28}$$

$$f_i^a=\int_{\Gamma_t}R_i^T H b\, d\Omega+\int_{\Omega^e}R_i^T H\bar{t}\, d\Gamma \tag{29}$$

$$f_i^{ba}=\int_{\Omega^e}R_i^T\beta_\alpha b\, d\Omega+\int_{\Gamma_t}R_i^T\beta_\alpha\bar{t}\, d\Gamma \tag{30}$$

$$f_i^c=\int_{\Omega^e}R_i^T H b\, d\Omega+\int_{\Gamma_t}R_i^T H\bar{t}\, d\Gamma\,, f_i^d=\int_{\Omega^e}R_i^T\psi(\xi) b\, d\Omega+\int_{\Gamma_t}R_i^T\psi(\xi)\bar{t}\, d\Gamma \tag{31}$$

Here, R_i^T symbolizes the NURBS basis function, and $B_i^u, B_i^a, B_i^b, B_i^{b\alpha}, B_i^c$ and B_i^d correspond to the matrices of NURBS basis function derivatives and are given by:

$$B_i^u=\begin{bmatrix} R_{i,x_1} & 0 \\ 0 & R_{i,x_2} \\ R_{i,x_2} & R_{i,x_1} \end{bmatrix}_{3\times n_{en}} \tag{32}$$

$$B_i^a=\begin{bmatrix} (R_i)_{,x_1}H & 0 \\ 0 & (R_i)_{,x_2}H \\ (R_i)_{,x_2}H & (R_i)_{,x_1}H \end{bmatrix} \tag{33}$$

$$B_i^b=[B_i^{b1} \quad B_i^{b2} \quad B_i^{b3} \quad B_i^{b4}] \tag{34}$$

$$B_i^{b,\alpha}=\begin{bmatrix} (R_i\beta_\alpha)_{,x_1} & 0 \\ 0 & (R_i\beta_\alpha)_{,x_2} \\ (R_i\beta_\alpha)_{,x_2} & (R_i\beta_\alpha)_{,x_1} \end{bmatrix}_{3\times n_{en}} \tag{35}$$

$$B_i^c=\begin{bmatrix} (R_i)_{,x_1}\chi & 0 \\ 0 & (R_i)_{,x_2}\chi \\ (R_i)_{,x_2}\chi & (R_i)_{,x_1}\chi \end{bmatrix}_{3\times n_{en}} \tag{36}$$

$$B_i^d=\begin{bmatrix} (R_i\psi)_{,x_1} & 0 \\ 0 & (R_i\psi)_{,x_2} \\ (R_i\psi)_{,x_2} & (R_i\psi)_{,x_1} \end{bmatrix}_{3\times n_{en}} \tag{37}$$

where, $\alpha=1,2,3,4$ and $r,s=u,a,b,c,d$

3. Result and discussion

3.1 Model Geometry, Boundary Conditions and Material Properties of Plate

To demonstrate the reliability and effectiveness of XIGA in evaluating Stress Intensity Factors (SIF), we conducted an analysis on specimens with single-edge, center, and double-edge cracks shown in the **Fig. (5).** In **Fig. (5)**, the top edge experiences a tensile load of $\sigma_o = 100MPa$, while the bottom edge is fixed in the y direction. The dimensions and material properties of the specimens are provided in **Table 1**.

Table 1. Dimensions and material attributes

Geometric Properties	Material Attributes
Length (L) = 1 cm, Height (2D) = 2 cm,	Modulus of Elasticity (E) $= 200 \times 10^3$GPa Poisson's ratio (ν) = 0.3

3.2 Single Edge Crack modeling using XIGA

In this first example, we examined a plate that contains a crack along one of its edges and is subjected to tensile loading, as depicted in **Fig. 4**.

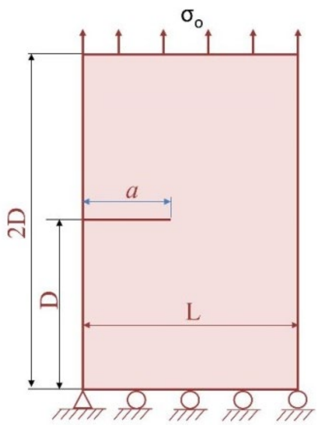

Fig. 4 Single edge crack boundary conditions and Dimensions

In this study, we applied XIGA to investigate the relationship between SIF I (KI) and crack length. The results obtained from XIGA were compared with those from XFEM and a closed form solution presented in reference Tada et al. (2000). The closed form solution used in the comparison is given by the equation:

$$K_I = f\sigma_o\sqrt{\pi a} \tag{38}$$

$$f = 1.122 - 0.231\left(\frac{a}{L}\right) + 10.55\left(\frac{a}{L}\right)^2 - 21.71\left(\frac{a}{L}\right)^3 + 30.382\left(\frac{a}{L}\right)^4 \tag{39}$$

where f is an empirical function, σ_o represents the applied tensile load, L is the plate width and a denotes the crack length.

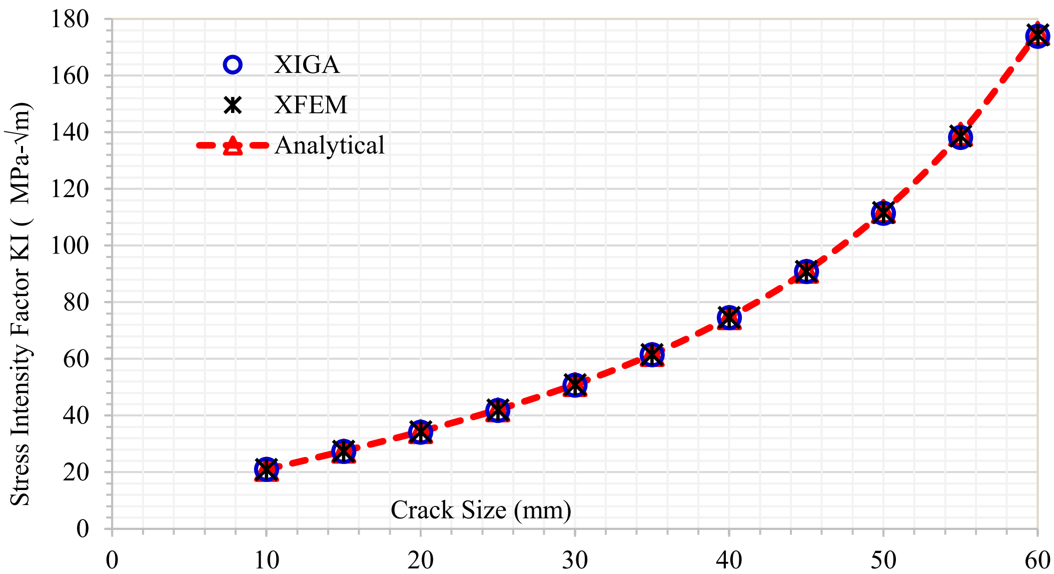

Fig. 5 Comparative study on the variation of SIF K_I with crack length

Fig. 6 presents the results for the model with a single-edge crack, demonstrating good agreement between the results obtained by XIGA with those from XFEM, and the closed form solutions. Furthermore, we evaluated the normalized SIF values and compared them with those from XFEM and the literature Yan (2007). The comparison, as depicted in **Fig. 7**, shows close agreement with minimal error. These findings indicate a positive correlation between the different solution methods, with a maximum error of 0.57%. Therefore, we conclude that XIGA is capable of capturing stress and deformation fields at the crack tips with reasonable accuracy.

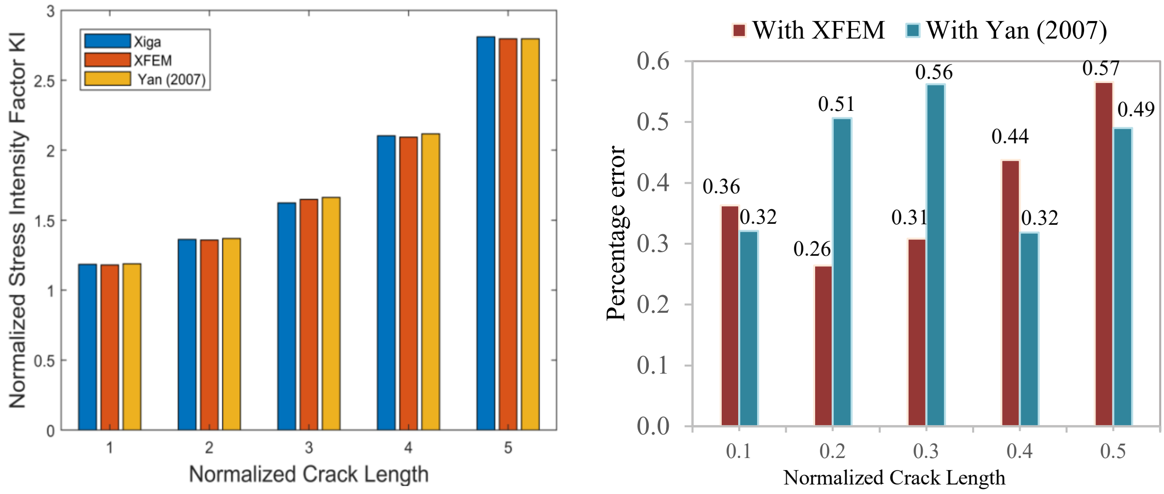

a) Normalized SIF with normalized crack length b) Percentage error comparison

Fig. 6 Comparison of SIF values from different methods

Additionally, **Fig. 7** illustrates the error estimation and convergence of mode-I SIF as a function of number of nodes. The plot confirms that as the number of nodes increases, the analytical value is approached, and the percentage error decreases.

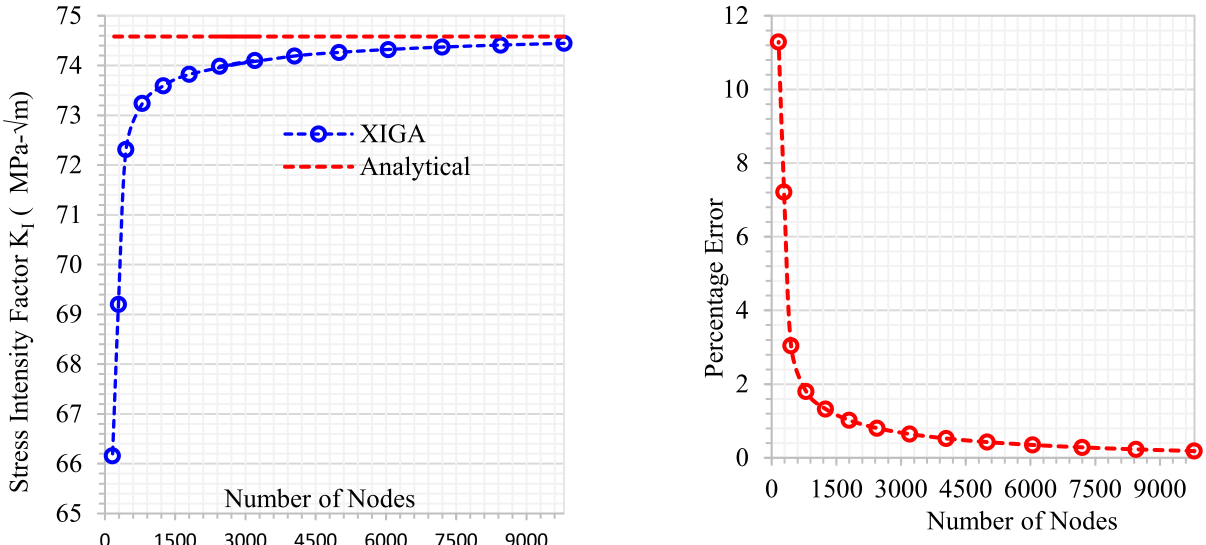

a) Convergence of KI as the number of nodes increased b) Percentage error with respect to number of nodes

Fig. 7 Convergence of K_I values from XIGA to closed form solution as a function of number of nodes

In this example we also conducted a parametric study on SIF KI for different values of applied load (σ_o) to establish the effectiveness of XIGA. A plot of SIF against the applied load (σ_o) is shown in **Fig. 8** below. The results obtained from XIGA show a strong agreement with the closed-form solutions Tada et al. (2000).

The plot of stress contours $\sigma_{xx}, \sigma_{xy}, \sigma_{yy}$ and displacement contour are illustrated in **Fig. 9 (a), (b), (c)** and **Fig. 9(d)** respectively. As it is expected maximum stress fields are observed at the crack tip and maximum displacement field is at the top left edge.

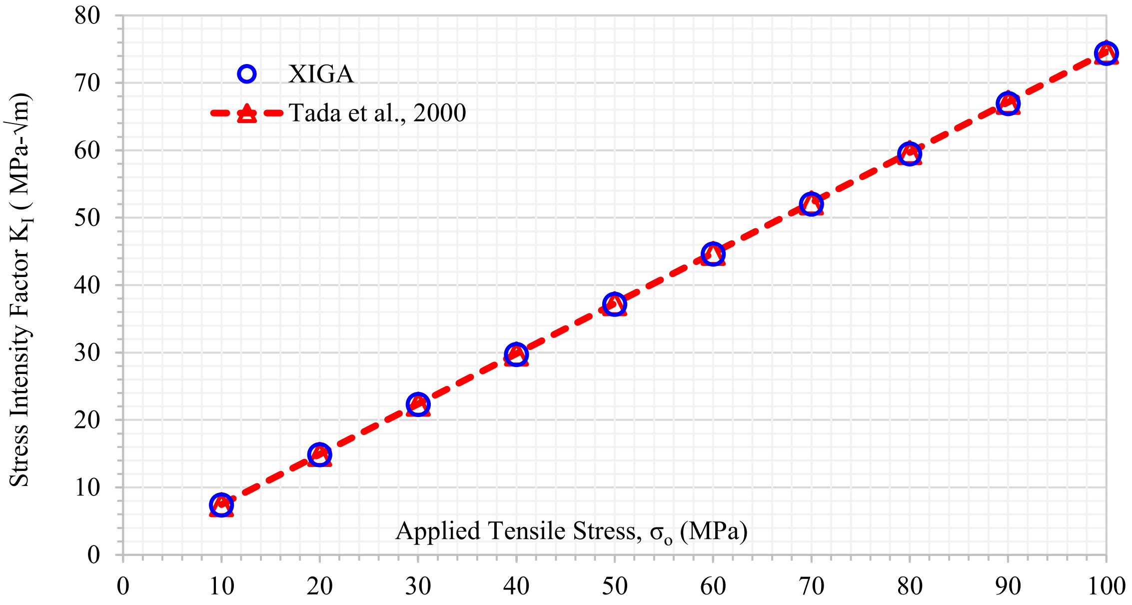

Fig. 8 Correlation between K_I and tensile stresses for a single edge cracked plate

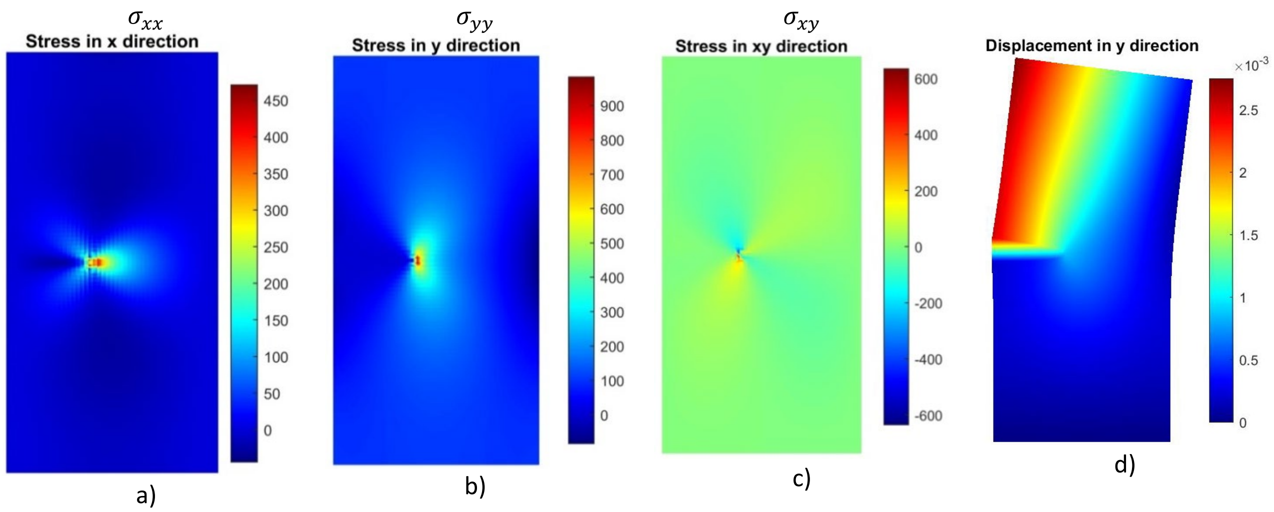

Fig. 9. Stress and displacement contour for an edge cracked plate

3.3 Double Edge Crack modeling using XIGA

In this analysis, we investigate a tension plate featuring a double-edge crack, as illustrated in **Fig. 10**. The loading condition and material properties are consistent with those used in example one.

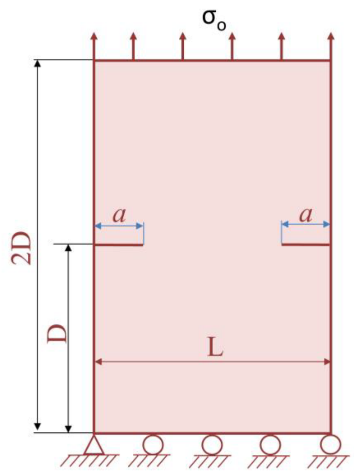

Fig. 10. Double edge crack boundary conditions and Dimensions

We explored how the Stress Intensity Factor I (K_I) varies in relation to the crack length through our analysis employing XIGA. The obtained results are compared with a closed form solution from reference Tada et al. (2000) as follows:

$$K_I = f\sigma_o\sqrt{\pi a} \tag{40}$$

$$f = 1.12 + 0.43\left(\frac{a}{L}\right) - 4.79\left(\frac{a}{L}\right)^2 + 15.46\left(\frac{a}{L}\right)^3 \tag{41}$$

Upon observing **Fig. 11**, it is evident that the results obtained from XIGA align satisfactorily with the analytical solutions Tada et al. (2000).

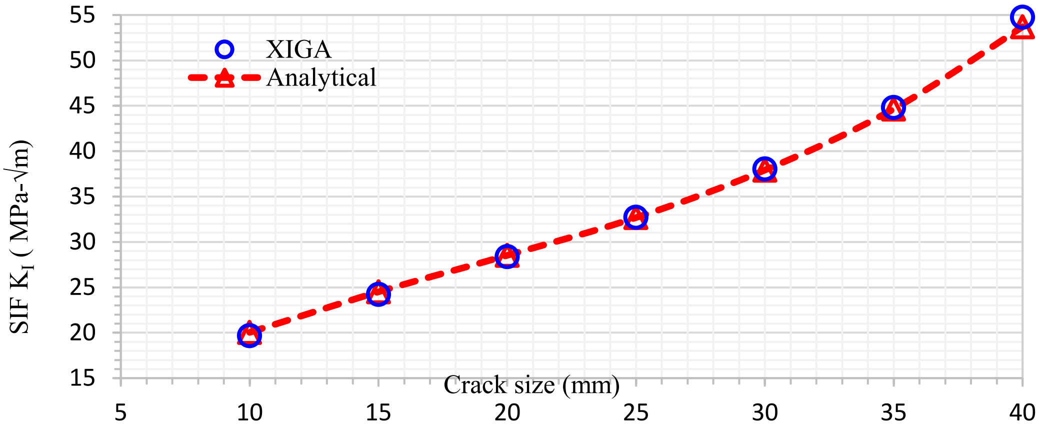

Fig. 11. variation of SIF K_I with crack length

We also examined the effect of the applied load (σ_o) on SIF K_I, as illustrated in **Fig. 12** to demonstrate the usefulness of XIGA. In **Fig. 12**, the SIF is plotted against the applied load (σ_o). The results obtained from XIGA exhibit good agreement with the analytical solutions presented in reference Tada et al. (2000).

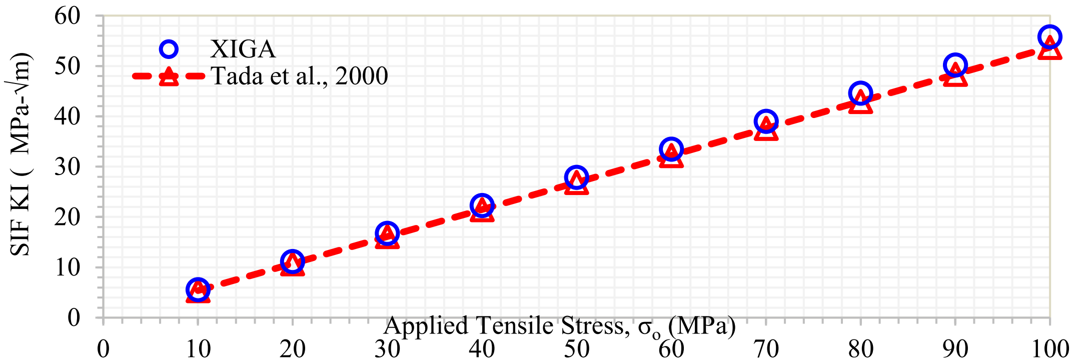

Fig. 12. variation of K_I with tensile stresses for a double edge cracked plate

Furthermore, **Fig. 13 (a), (b), (c),** and **Fig. 13(d)** display the stress contours $\sigma_{xx}, \sigma_{yy}, \sigma_{xy}$ and displacement respectively. As anticipated, the stress-fields are highest at the crack-tip, while the displacement field reaches its maximum at the top edge.

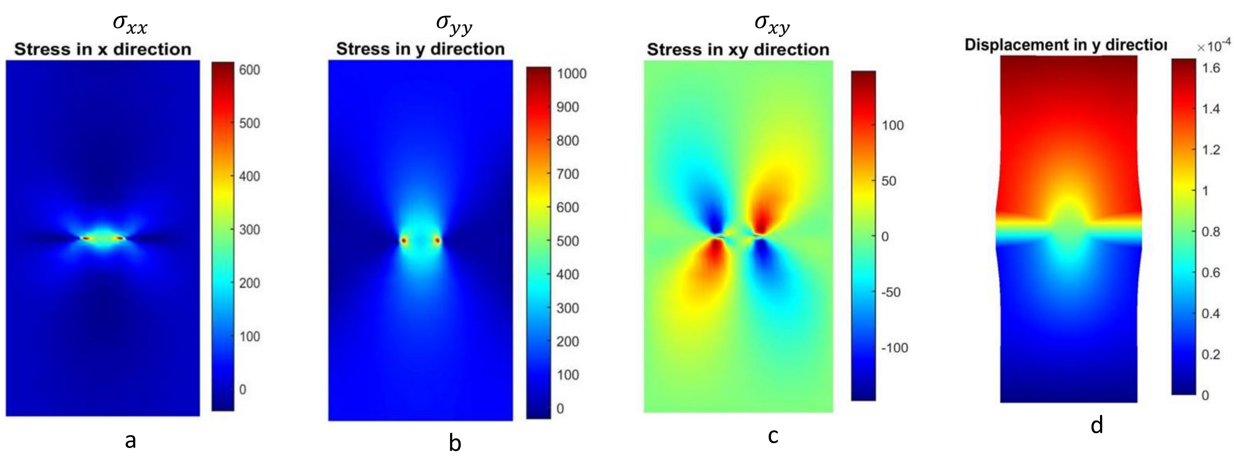

Fig. 13. Stress and displacement contour for double edge cracked plate

3.4 Center Crack modeling using XIGA

In this particular case, we examine a tension plate featuring a crack positioned at the center, as illustrated in **Fig. 14**. The loading condition and material properties are similar to those in examples one and two.

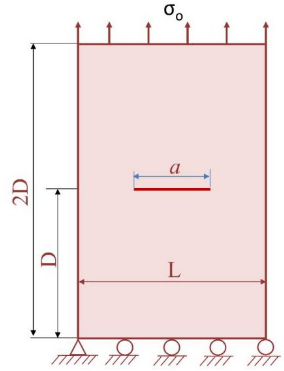

Fig. 14 Central crack boundary conditions and Dimensions

Through the use of XIGA, we analyze the relationship between the Stress Intensity Factor I (K_I) and the crack length. The closed form solution for K_I is approximated from reference Tada et al. (2000) as follows:

$$K_I = f\sigma_o\sqrt{\pi a} \tag{42}$$

$$f = \sqrt{\sec\frac{\pi a}{W}} \tag{43}$$

The results obtained from XIGA demonstrate a strong agreement with the analytical solutions Tada et al. (2000) as it is shown in **Fig. 15.**

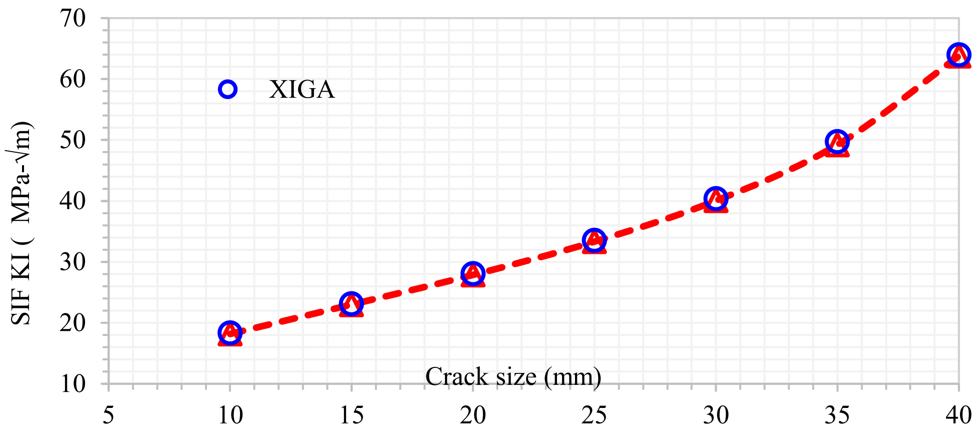

Fig. 15 variation of SIF K_I with crack length

Additionally, we examine the effect of the applied load (σ_o) on SIF K_I, as illustrated in **Fig. 16**, to demonstrate the usefulness of XIGA. In **Fig. 16**, the SIF is plotted against the applied load (σ_o). It is evident that the results obtained from XIGA align well with the analytical solutions (Tada et al., 2000).

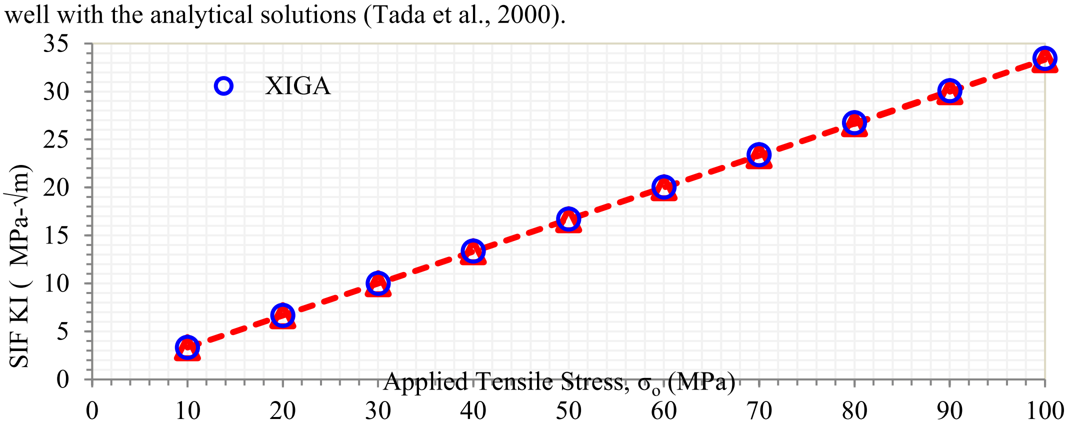

Fig. 16 variation of KI with tensile stresses for centrally cracked plate

Moreover, **Fig. 17 (a), (b),** and **Fig. 17 (c)** show the stress contours σ_{xx}, σ_{yy} and σ_{xy} respectively. As expected, the stress fields are highest at the crack tip.

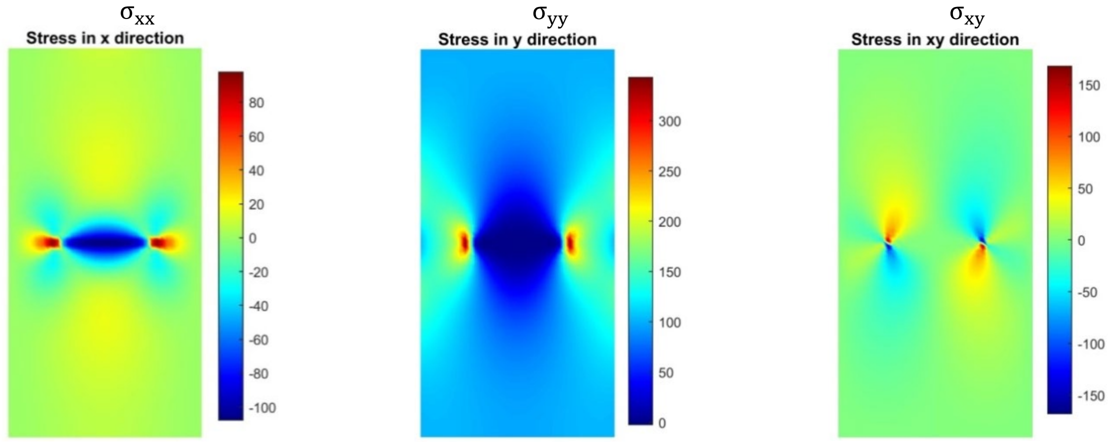

a b c

Fig. 17. Stress and displacement contour for centrally cracked plate

3.5 Edge Crack in Shear Loading using XIGA

This example demonstrates the versatility of XIGA approach in dealing with the mixed-mode SIFs K_I and K_{II}. An edge-cracked plate subjected to a uniform shear stress of τ = 100 MPa, as shown in Fig. 18, has been examined using similar geometry and material properties as in the previous example.

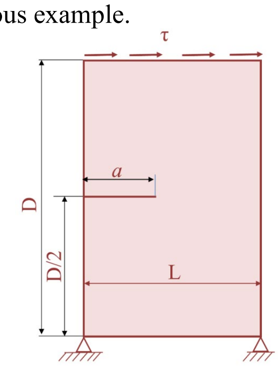

Fig. 18. Edge-cracked plate with boundary conditions and Dimensions

Fig. 19 below shows the mixed mode SIF results (K_I and K_{II}) against the crack size from the analysis of an edge cracked plate subjected to shear using XIGA. As the crack moves the both K_I and K_{II} increase as we expect.

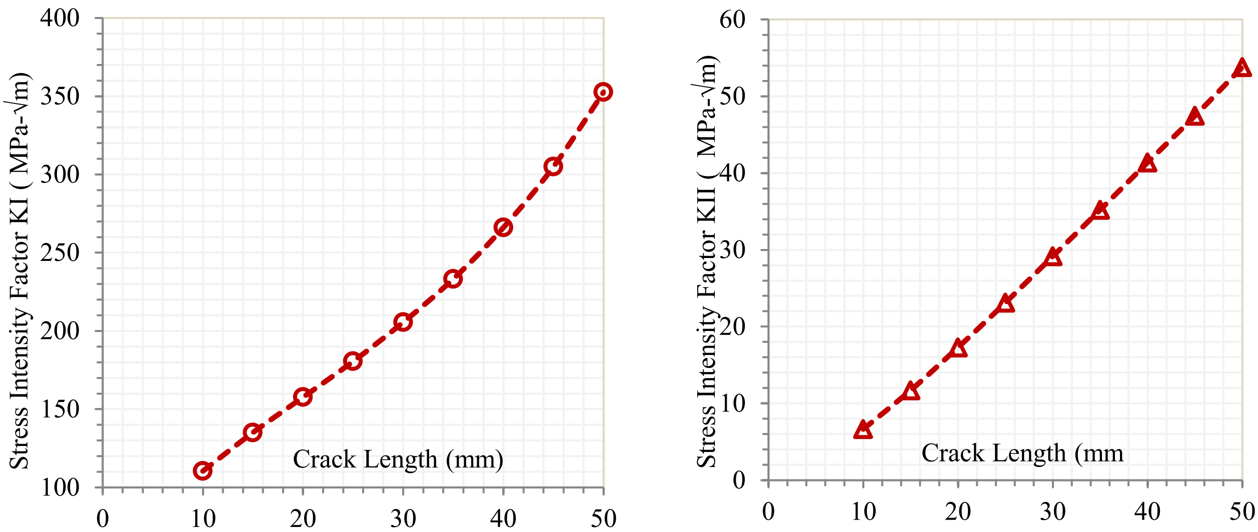

a) variation of SIF K_I with crack length b) variation of SIF K_{II} with crack length

Fig. 19. Mixed-mode SIFs result from XIGA against crack length

Fig. 20 illustrates the convergence of mode-I (K_I) and Mode II (K_{II}) SIFs as a function of number of nodes. The plot confirms that as the number of nodes increases, the analytical value is approached.

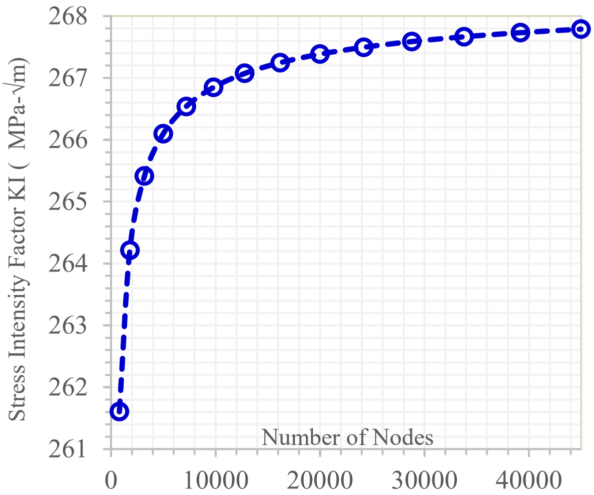

c) Convergence of K_I as the number of nodes increased

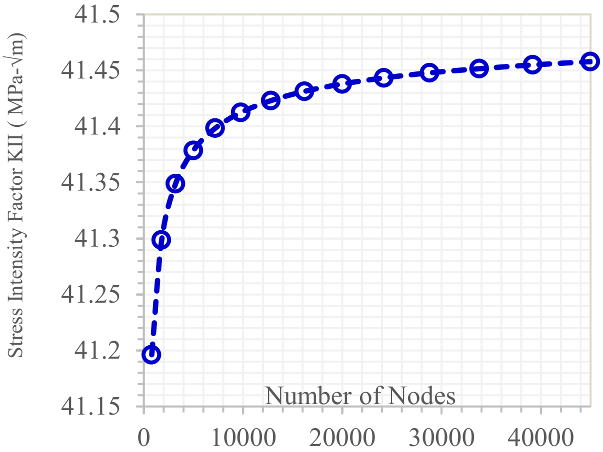

d) Convergence of K_{II} as the number of nodes increased

Fig. 20. Convergence of K_I and K_{II} values from XIGA as a function of number of nodes

The example also examines the effect of the applied shear stress (τ) on the stress intensity factor (SIF) K_I, as illustrated in **Fig. 21.** This demonstrates the usefulness of the XIGA approach. In **Fig. 21**, the SIF is plotted against the applied shear stress (τ). The results obtained from the XIGA analysis align well with the analytical solutions of Tada et al. (2000), highlighting the accuracy and reliability of the XIGA approach.

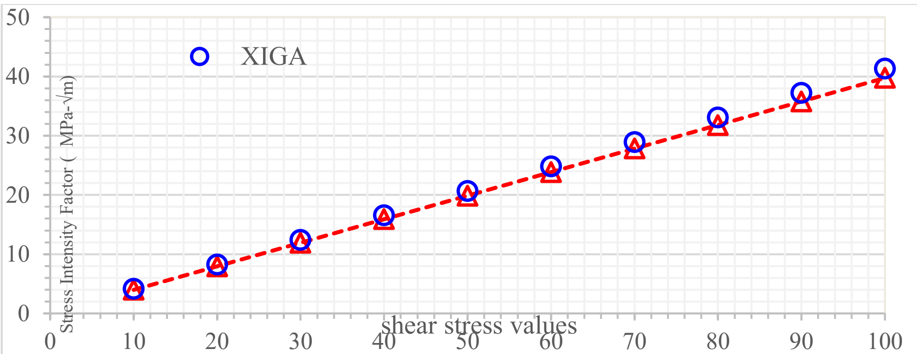

Fig. 21. variation of K_I with shear stresses for edge cracked plate

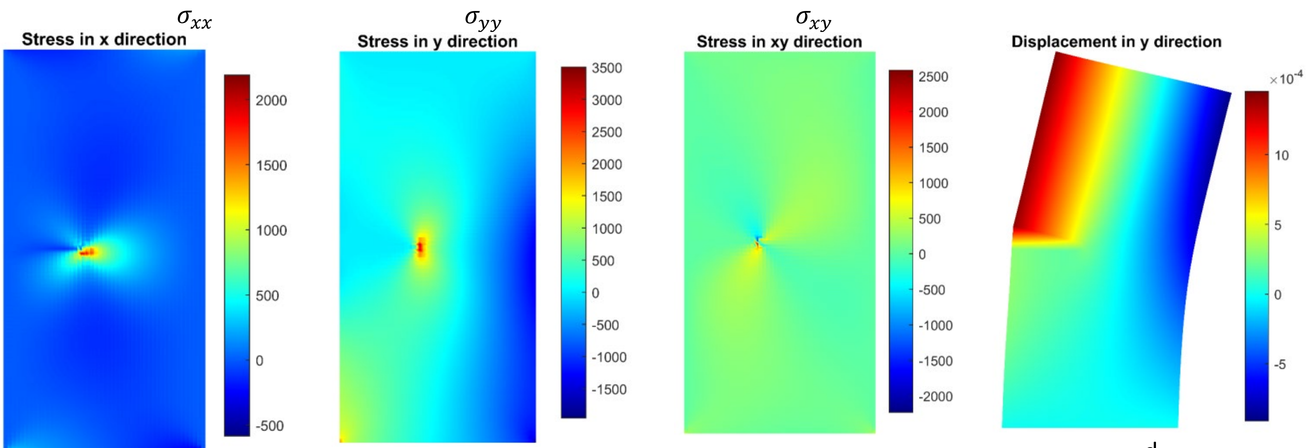

a b c d

Fig. 22 Stress and displacement contour for an edge cracked plate in shear

Additionally, **Fig. 22(a), (b),** and **Fig. 22(c)** showcase the stress contour plots for the normal stress components σ_{xx} and σ_{yy} as well as the shear stress component σ_{xy} respectively. As we expect based on the fundamental principles of fracture mechanics, the stress fields are expected to reach their peak values in the immediate vicinity of the crack tip region. This is a well-established phenomenon, as the presence of a crack tip introduces a localized stress singularity, leading to the elevated stress levels in that critical area of the structural component.

4. Conclusion

In this study, we employed XIGA to analyze tension plates with single-edge, center, and double-edge cracks. NURBS basis function has been implemented for the geometry and solution. The results obtained from XIGA were compared with analytical solutions, results from literatures and XFEM, demonstrating the reliability and effectiveness of XIGA in evaluating Stress Intensity Factors (SIF). The agreement between XIGA, XFEM, and the closed form solutions was found to be excellent, with minimal error. This indicates that XIGA is capable of accurately capturing stress and deformation fields at crack tips. Additionally, a parametric study on SIF K_I for different applied loads further confirmed the effectiveness of XIGA. The stress contours and displacement fields obtained from XIGA were consistent with expectations, with maximum stress observed at the crack tip and maximum displacement at the top edge. Based on the positive outcomes of this study, we recommend the utilization of XIGA for analyzing stress and deformation fields in cracked plates. Its accurate determination of Stress Intensity Factors makes it a valuable tool in fracture mechanics studies. Researchers and engineers can confidently rely on XIGA to obtain reliable results and gain insights into the behavior of cracked structures.

References

Belytschko, T., & Black, T. (1999). Elastic crack growth in finite elements with minimal remeshing. *International journal for numerical methods in engineering*, *45*(5), 601-620.

Belytschko, T., Gu, L., & Lu, Y. Y. (1994, a). Fracture and crack growth by element free Galerkin methods. *Modelling and Simulation in Materials Science and Engineering*, *2*(3A), 519.

Belytschko, T., Lu, Y. Y., & Gu, L. (1994, b). Element-free Galerkin methods. *International journal for numerical methods in engineering*, *37*(2), 229-256.

Bhardwaj, G., Singh, S. K., Patil, R. U., Godara, R. K., & Khanna, K. (2021). Thermo-elastic analysis of cracked functionally graded materials using XIGA. *Theoretical and Applied Fracture Mechanics*, 114, 103016.

Borden, M. J., Verhoosel, C. V., Scott, M. A., Hughes, T. J., & Landis, C. M. (2012). A phase-field description of dynamic brittle fracture. *Computer Methods in Applied Mechanics and Engineering*, *217*, 77-95.

Bouhala, L., Shao, Q., Koutsawa, Y., Younes, A., Núñez, P., Makradi, A., & Belouettar, S. (2013). An XFEM crack-tip enrichment for a crack terminating at a bi-material interface. *Engineering Fracture Mechanics*, *102*, 51-64.

Ching, H. K., & Yen, S. C. (2005). Meshless local Petrov-Galerkin analysis for 2D functionally graded elastic solids under mechanical and thermal loads. *Composites Part B: Engineering*, *36*(3), 223-240.

De Luycker, E., Benson, D. J., Belytschko, T., Bazilevs, Y., & Hsu, M. C. (2011). X-FEM in isogeometric analysis for linear fracture mechanics. *International Journal for Numerical Methods in Engineering*, *87*(6), 541-565.

Fang, W., Zhang, J., Yu, T., & Bui, T. Q. (2021). Analysis of thermal effect on buckling of imperfect FG composite plates by adaptive XIGA. *Composite Structures*, 275, 114450.

Ghorashi, S. S., Valizadeh, N., & Mohammadi, S. (2012). Extended isogeometric analysis for simulation of stationary and propagating cracks. *International Journal for Numerical Methods in Engineering*, *89*(9), 1069-1101.

Grifith, A. A. (1920). The phenomena of rupture and flow in solids. *Phil. Trans. R. Soc. Lond., A*, *221*, 163.

Gu, J., Yu, T., Tanaka, S., Qiu, L., & Bui, T. Q. (2019). Adaptive orthotropic XIGA for fracture analysis of composites. *Composites Part B: Engineering*, 176, 107259.

Gu, Y., Wang, W., Zhang, L. C., & Feng, X. Q. (2011). An enriched radial point interpolation method (e-RPIM) for analysis of crack tip fields. *Engineering Fracture Mechanics*, *78*(1), 175-190.

Hughes, T. J., Cottrell, J. A., & Bazilevs, Y. (2005). Isogeometric analysis: CAD, finite elements, NURBS, exact geometry and mesh refinement. *Computer methods in applied mechanics and engineering*, *194*(39-41), 4135-4195.

Irwin, G. R. (1957). Analysis of stresses and strains near the end of a crack traversing a plate.

Jameel, A., & Harmain, G. A. (2019). Extended iso-geometric analysis for modeling three-dimensional cracks. *Mechanics of Advanced Materials and Structures*, *26*(11), 915-923.

Kastratović, G., Vidanović, N., Grbović, A., & Rašuo, B. (2018). Approximate determination of stress intensity factor for multiple surface cracks. *FME transactions*, *46*(1), 39-45.

Lee, S. H., Kim, K. H., & Yoon, Y. C. (2016). Particle difference method for dynamic crack propagation. *International Journal of Impact Engineering*, *87*, 132-145.

Liu, W. K., Jun, S., & Zhang, Y. F. (1995). Reproducing kernel particle methods. *International journal for numerical methods in fluids*, *20*(8-9), 1081-1106.

Lu, Y. Y., Belytschko, T., & Gu, L. (1994). A new implementation of the element free Galerkin method. *Computer methods in applied mechanics and engineering*, *113*(3-4), 397-414.

Menk, A., & Bordas, S. P. (2011). Crack growth calculations in solder joints based on microstructural phenomena with X-FEM. *Computational Materials Science*, *50*(3), 1145-1156.

Miehe, C., Hofacker, M., & Welschinger, F. (2010, a). A phase field model for rate-independent crack propagation: Robust algorithmic implementation based on operator splits. *Computer Methods in Applied Mechanics and Engineering*, *199*(45-48), 2765-2778.

Miehe, C., Welschinger, F., & Hofacker, M. (2010, b). Thermodynamically consistent phase-field models of fracture: Variational principles and multi-field FE implementations. *International journal for numerical methods in engineering*, *83*(10), 1273-1311.

Moës, N., Dolbow, J., & Belytschko, T. (1999). A finite element method for crack growth without remeshing. *International journal for numerical methods in engineering*, *46*(1), 131-150.

Nguyen, V. P., Anitescu, C., Bordas, S. P., & Rabczuk, T. (2015). Isogeometric analysis: an overview and computer implementation aspects. *Mathematics and Computers in Simulation*, *117*, 89-116.

Pais, M. J. (2011). *Variable amplitude fatigue analysis using surrogate models and exact XFEM reanalysis*. University of Florida.

Rabczuk, T., & Belytschko, T. (2004). Cracking particles: a simplified meshfree method for arbitrary evolving cracks. *International journal for numerical methods in engineering*, *61*(13), 2316-2343.

Shoheib, M. M. (2023). Stress intensity factor and fatigue life evaluation for important points of semi-elliptical cracks in welded pipeline by Bezier extraction based XIGA and new correlation model. *Engineering Analysis with Boundary Elements*, 155, 264-280.

Sih, G. C. (1973). *Handbook of stress-intensity factors*. Lehigh University, Institute of Fracture and Solid Mechanics.

Singh, I. V., Mishra, B. K., Bhattacharya, S., & Patil, R. U. (2012). The numerical simulation of fatigue crack growth using extended finite element method. *International Journal of Fatigue*, *36*(1), 109-119.

Tada, H., Paris, P. C., & Irwin, G. R. (2000). The stress analysis of cracks Handbook (3rd ed.), ASME Press, New York.

Yan, X. (2007). Rectangular tensile sheet with single edge crack or edge half-circular-hole crack. *Engineering Failure Analysis*, *14*(7), 1406-1410.

Yang, H. S., Dong, C. Y., Qin, X. C., & Wu, Y. H. (2020). Vibration and buckling analyses of FGM plates with multiple internal defects using XIGA-PHT and FCM under thermal and mechanical loads. *Applied Mathematical Modelling*, 78, 433-481.

Zeleke, M., Dintwa, E., & Nwaigwe, K. (2021). Stress intensity factor computation of inclined cracked tension plate using XFEM. *Engineering Solid Mechanics*, *9*(4), 363-376.

Zhong, S., Jin, G., Ye, T., & Chen, Y. (2024). A 3D-XIGA rotating cracked model for vibration analysis of blades. *International Journal of Mechanical Sciences*, 261, 108700.